FULL PAPER

Relationship between pressure variations at the ocean bottom and the acceleration of its motion during a submarine earthquake

Mikhail Nosov[1,2], Viacheslav Karpov[1*], Sergey Kolesov[1], Kirill Sementsov[1], Hiroyuki Matsumoto[3] and Yoshiyuki Kaneda[4]

Abstract

The data provided by ten DONET deep-sea observatories, that on March 11, 2011, registered the Great East Japan Earthquake and tsunami, were used for investigation of the relationship between variations of the ocean bottom pressure and three-component accelerograms. Methods of cross-spectral analysis revealed the existence of a frequency range of "forced oscillations," within which pressure variations are proportional to the vertical component of the acceleration. This proportionality is manifested by the magnitude-squared coherence (MSC) being close to unity and a phase lag (PL) practically equal to zero. The spectral analysis method showed the proportionality coefficient to be equal the mass of a water column of unit area at the installation point of the observatory or, approximately, to the product of the water density and the ocean depth. The observed boundaries of the frequency range of "forced oscillations" are revealed to correspond to the theoretical frequency values confining the manifestation of surface gravity and acoustic waves in pressure variations near the ocean bottom. The hypothesis is put forward that the small deviations of MSC from unity and of PL from zero observed by a number of stations within the range of "forced oscillations" are due to the contribution of horizontal movements of nearby submarine slopes. A theoretical analysis has been performed of the problem of forced oscillations of a water layer in a basin of varying depth. A formula is obtained that relates pressure variations at the ocean bottom to acceleration components of the bottom motion and the bottom slope. The pressure in the region of forced oscillations is shown to decrease exponentially with the distance from the moving segment of the ocean bed, so pressure variations, originating from movements of the bottom, are registered effectively by a gauge at the ocean bottom only within a radius less than 1–2 ocean depths. A cross-spectral analysis of pressure variations and of three-component accelerograms confirmed the hypothesis concerning the contribution of horizontal movements of nearby submarine slopes to pressure variations.

Keywords: Tsunami, DONET, Ocean bottom pressure, Ocean bottom acceleration, Cross-spectrum, The 2011 Tohoku earthquake

Introduction

Till the second half of the Twentieth century, earthquakes and tsunamis were only registered by land-based seismic stations and coastal mareographs. The development of ocean bottom seismology—not to consider individual early experiments, e.g., (Ewing and Vine 1938)—originated in the 1960s (Bradner 1964). The "hydrophysical" method of tsunami forecasting, based on pressure gauges installed at the ocean bottom detecting waves at long distances from the coast (Soloviev 1968; Jaque and Soloviev 1971), was proposed at about the same time. At present, upon having undergone significant technical development, deep-water measurements are actively applied for

*Correspondence: va.karpov@physics.msu.ru
[1] Chair of Physics of Sea and Inland Water, Faculty of Physics, M.V.Lomonosov Moscow State University, Moscow, Russia 119991
Full list of author information is available at the end of the article

Nosov *et al. Earth, Planets and Space* (2018) 70:100

Page 2 of 13

monitoring earthquakes and tsunamis (Suetsugu and Shiobara 2014; Rabinovich and Eblé 2015).

Of modern deep-water tsunami detectors the most renowned among professionals is the DART (deep-ocean assessment and reporting of tsunamis) system that at present involves about 60 stations installed in different regions of the World ocean (Rabinovich and Eblé 2015; Levin and Nosov 2016). Moreover, various regional deep-water devices for measuring the sea level, such as, for example, DONET (dense oceanfloor network system for earthquakes and tsunamis) (Kaneda 2010), NEPTUNE (The Canadian North-East Pacific Underwater Networked Experiments) (Barnes and Team 2007), EMSO (European Multidisciplinary Seafloor and water column Observatory) (Favali and Beranzoli 2009) and others, are in operation.

In comparison with coastal mareographs, deep-water tsunami detectors exhibit a whole series of advantages, among which we primarily single out their advance time in revealing a wave and the invulnerability of their measuring systems to the destructive effect of catastrophic tsunamis (Titov et al. 2005; Levin and Nosov 2016). Perhaps, the only serious defect of deep-water tsunami detectors consists in noise pollution of the signal due to manifestations of seismic and hydroacoustic waves. The level of such noise in the vicinity of a seismic source may exceed the level of the tsunami signal by several orders of magnitude (Watanabe et al. 2004; Nosov and Kolesov 2007). An understanding of the physical processes resulting in the formation of signals, registered by seafloor pressure gauges, is very important for correct identification of the tsunami signal aimed at its further application in resolving problems of early tsunami warning (Nosov and Grigorieva 2015; Gusman et al. 2016; Takahashi et al. 2017).

The peculiarities and nature of signals registered by measuring devices at the ocean bottom were discussed in refs. (Filloux 1983; Webb 1998) on the basis of on-site data, available by the end of the twentieth century. The unflagging interest in the problem is demonstrated by a recent publication (An et al. 2017), in which a theoretical analysis is presented of regularities in the formation of pressure variations at the flat bottom of an incompressible ocean and an analysis of modern on-site data is performed.

The 2003 Tokachi-oki earthquake happened to be the first tsunamigenic event with its epicenter in the immediate vicinity of gauges of the seafloor observatory Kushiro-Tokachi/JAMSTEC (Watanabe et al. 2004). Analysis of its data resulted in significant progress in understanding the properties of signals registered by seafloor observatories (Watanabe et al. 2004; Nosov et al. 2005; Nosov and Kolesov 2007; Li et al. 2009; Ohmachi and Inoue 2010;

Bolshakova et al. 2011). Regretfully, peculiarities of the installation of pressure gauges of the Kushiro-Tokachi station hindered interpretation of the results of measurements. The point is that the pressure gauges and the seismometers were located at a significant distance from each other ($\sim$ 4 km) and, moreover, there existed an uncertainty in the orientation of the accelerometer axes. The DONET-1 system of seafloor observatories deployed by JAMSTEC in 2006–2011 turned out to be free of the above defects. Each DONET-1 observatory is equipped with an ocean bottom seismometer-(OBS), and a pressure gauge-(PG), situated at practically the same point, and the orientation of seismometers is rigorously calibrated (Nakano et al. 2012; Matsumoto et al. 2017).

By the time, the Great East Japan Earthquake (the 2011 Tohoku earthquake) took place 10 stations of the DONET-1 network were in operation—they all successfully recorded both the actual seismic event and the subsequent tsunami waves. Earlier, we already investigated the low-frequency component ($f < 0.01$ Hz) of pressure variations registered by DONET-1 observatories for resolving a number of problems related to tsunami waves (Nosov and Grigorieva 2015; Nurislamova and Nosov 2016). The signals obtained by the PG and OBS (only the vertical component) gauges of two DONET-1 observatories (B08, C09) were investigated in refs. (Matsumoto et al. 2017; Levin and Nosov 2016).

In this work, we present an analysis of the complete set of data (pressure variations and three-component accelerograms), registered by DONET-1 observatories during the 2011 Tohoku earthquake. In the work, we put an accent on the relationship between ocean bottom pressure variations and accelerations in movements of the ocean bottom, following from on-site observed data, and, also, on the physical interpretation and development of a mathematical model of this phenomenon. Special attention is devoted to a discussion of the contribution of horizontal components of the acceleration of the ocean bottom movement to pressure variations at the ocean bottom.

Description of the on-site data

The Great East Japan Earthquake took place on March 11, 2011, at 05:46 UTC. According to JMA (Japan Meteorological Agency) data, its epicenter was located at the point with coordinates 38.322N, 142.369E, while its moment magnitude amounted to $M_w = 9.0$ (JMA 2011). The disposition of the ten DONET-1 observatories that registered this event is shown in Fig. 1. The distribution of depths and ocean bottom inclinations, presented in Fig. 1, are based on JODC-Expert Grid data for Geography (J-EGG500).

Nosov *et al. Earth, Planets and Space* (2018) 70:100

Page 3 of 13

Each DONET-1 observatory is equipped with a block for measuring pressure (quartz PG Paroscientific and differential PG Nichiyu Giken) and a seismoblock located at a distance not greater than 10 m from each other. The seismoblock includes two seismometers: a broadband velocimeter (Guralp CMG-3T) and an accelerometer (Metrozet TSA-100S) (Araki et al. 2013). In spite of the DONET-1 observatories being located at a large distance from the epicenter (750 km), the strength of the earthquake was so great that the broadband velocimeters happened to be saturated, which resulted in only data from the accelerometers being useful.

In the further analysis, we shall use the three-hour records (from 05:30 UTC to 08:30 UTC of March 11, 2011), obtained by the PGs and the three-component OBS accelerometers. The frequency of digitizing data from the PGs was 10 Hz. The initial digitization frequency of seismic data was 200 Hz. To provide for the possibility of cross-spectral analysis, the accelerograms were downsampled to the frequency 10 Hz. The resulting length of each record amounted to 108,000 readouts.

In Fig. 2, we present the example of signals obtained by the A02 observatory. The main seismic event $M_w9.0$ and the first strong aftershock $M_w7.9$ clearly show up both in pressure variations at the ocean bottom and in each of the three components of the bottom acceleration. The double amplitude of pressure variations amounted to 87.5 kPa. The leading tsunami wave manifests itself in pressure variations about 1 h 15 min after the beginning of the earthquake with a significantly lower amplitude of 4 kPa (0.4 m). The peak values of acceleration components (double amplitude) amounted to 14.4, 17.5 and 6.5 cm/s^2 along the *x*, *y* and *z* axes, respectively.

Cross-spectral analysis

At the first stage of investigating the relationship between pressure variations and accelerations, we applied cross-spectral analysis (Bloomfield 2000). To reduce random errors in the "magnitude-squared coherence" (MSC) and the "phase lag" (PL), we made use of the mean values of these quantities. Averaging was performed by Welch's method (Bendat and Piersol 2010). Each time series was divided with the aid of the Hann window into 27 segments with a 50% overlap. The size of a segment amounted to 2^{13} readouts. The theoretical normalized random error of the estimate for squared coherence was 3.1×10^{-3}. The error was so small that it had no sense to show it in the plot.

Results of the cross-spectral analysis of pressure variations and of the vertical component of acceleration are presented in Fig. 3 by the blue curves. It is clearly seen that for each of the ten observatories there exists a frequency range (from about 0.02 up to 0.1 Hz), within
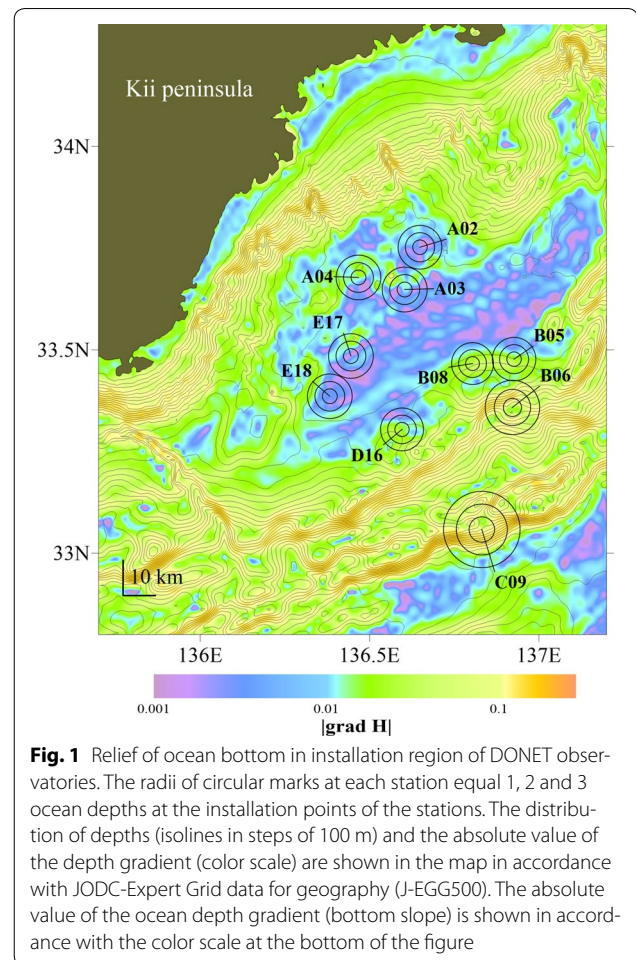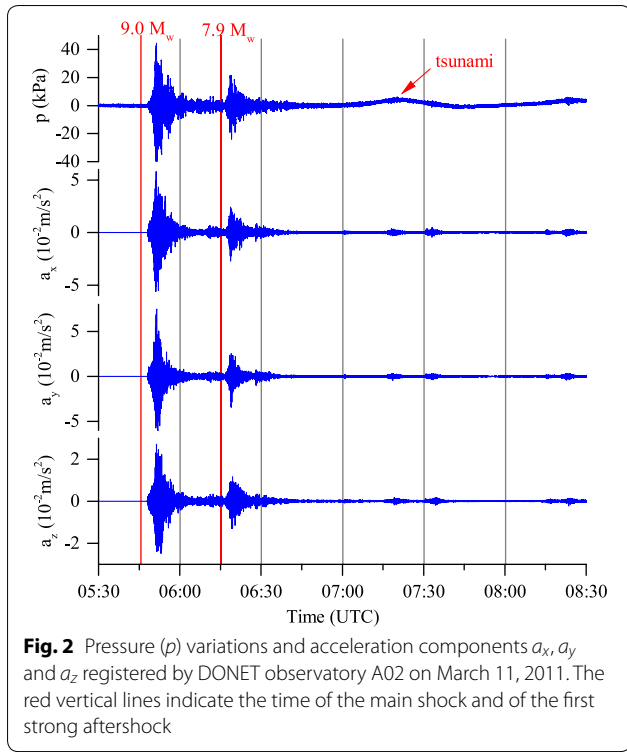

Fig. 1 Relief of ocean bottom in installation region of DONET observatories. The radii of circular marks at each station equal 1, 2 and 3 ocean depths at the installation points of the stations. The distribution of depths (isolines in steps of 100 m) and the absolute value of the depth gradient (color scale) are shown in the map in accordance with JODC-Expert Grid data for geography (J-EGG500). The absolute value of the ocean depth gradient (bottom slope) is shown in accordance with the color scale at the bottom of the figure

which the coherence (MSC) value is quite close to unity and the phase lag (PL) to zero. The observed character of cross-spectra reveals that within the frequency band indicated pressure variations are quite precisely proportional to the vertical acceleration component of the motion of the ocean bottom.

Careful examination of the cross-spectra shows that there are small deviations of the MSC from unity and of the PL from zero. These deviations are particularly noticeable in the case of observatories B06, B08 and C09, which were installed at sites of a sloped ocean bottom (see Fig. 1). Here, "perfect" cross-spectra (MSC = 1, PL = 0) are shown by signals registered by observatories A02, E17 and E18, that are installed on practically flat segments of the ocean bottom. The observed peculiarities exhibited by the cross-spectra suggest that deviations may be explained by the contribution to pressure variations of horizontal seismic movements of submarine slopes. This issue will be dealt with in greater detail in "Contribution of horizontal movements of the ocean bottom to near-bottom pressure variations" section.

Nosov *et al. Earth, Planets and Space* (2018) 70:100

Page 4 of 13

Fig. 2 Pressure (*p*) variations and acceleration components a_x, a_y and a_z registered by DONET observatory A02 on March 11, 2011. The red vertical lines indicate the time of the main shock and of the first strong aftershock

The linear relationship between pressure variations and the vertical component of the ocean bottom acceleration corresponds to Newton's second law written for a water column of unit area that undergoes vertical forced oscillations following movements of the ocean bottom,

$$p = \rho H a_z, \tag{1}$$

where ρ is the water density, H is the ocean depth, and a_z is the vertical acceleration component of the ocean bottom's motion. Formula (1) is mentioned in various publications (Filloux 1983; An et al. 2017), where the sole restriction to be imposed on its applicability consists in that the liquid is to be considered incompressible. Actually, from classical mechanics it follows that for formula (1) to be precise the water column must move like a solid-state body inseparably linked with the ocean bottom, and the quantity ρH must be considered as the mass of a water column of unit area.

The real ocean is not similar to the model object described, since vertical motion of its bottom not only excites forced oscillations in the water layer, but also

gravity and acoustic waves. The contribution of waves to pressure variations depends on regularities differing from formula (1). The contribution of surface gravity waves to oscillations of pressure at the ocean bottom is proportional to the amplitude of these waves, which, in turn, is proportional to the amplitude of bottom movements. On the other hand, the contribution of hydroacoustic waves is proportional to the motion velocity of the bottom. Thus, relation (1) can be expected to be satisfied accurately, only if neither gravity nor acoustic waves are excited by motion of the ocean bottom. Precisely such a situation is realized in the case of bottom oscillations within the frequency range $f_g < f < f_{ac}$, where f_g and f_{ac} are the limit frequency values for surface gravity and acoustic waves due to motion of the ocean bottom. The theoretical values of limit frequencies are determined by formulas (Levin and Nosov 2016; Matsumoto et al. 2017):

$$f_g = 0.366\sqrt{g/H},$$
$$f_{ac} = c/4H,$$

where g is the gravity acceleration and c is the speed of sound in water.

The theoretical values of limit frequencies f_g and f_{ac}, calculated for $g = 9.8$ m/s², $c = 1500$ m/s and ocean depths at installation points of the stations (the values are given in the figure) are indicated in Fig. 3 by vertical lines. The theoretical estimate for limit frequencies is seen to be in good agreement with the actually observed frequency range, within which the MSC is close to unity, and PL is close to zero. The frequency range $f_g < f < f_{ac}$ will further be termed the range of forced oscillations.
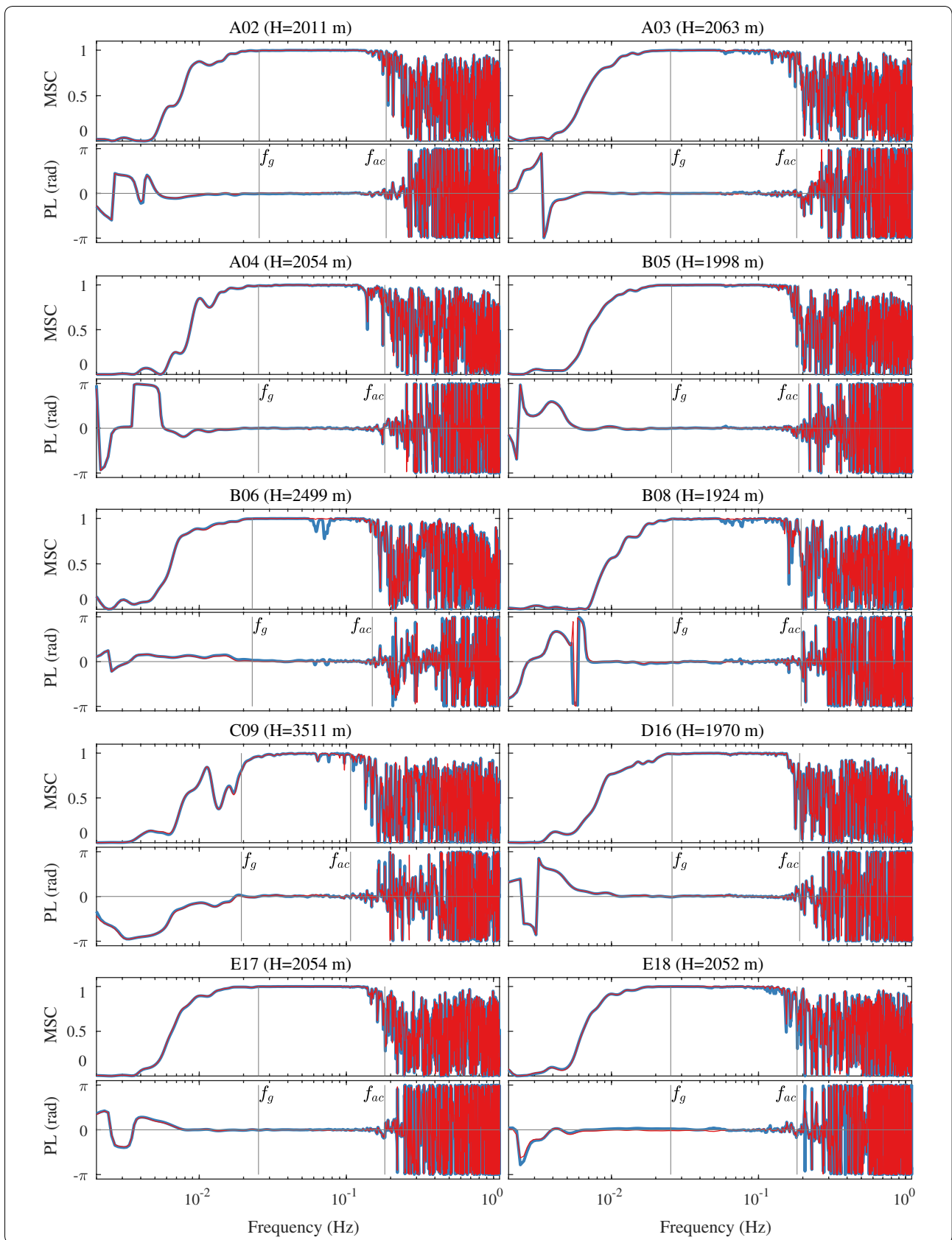
The deviations of MSC from unity and of PL from zero, observed in all cases at the higher-frequency end of the forced oscillation band, deserve a special comment. We think the nature of these deviations to be due to the compressibility of water. A compressible layer of water is known to represent a waveguide characterized by the dispersion relation (Tolstoy and Clay 1987):

$$k_x = \sqrt{\omega^2/c^2 - k_z^2},$$

where k_x is the horizontal wave number and $k_z = \pi(1 + 2n)/2H$ is the vertical wave number for the n-th mode (n = 0, 1, 2…), ω is the cyclic frequency

(See figure on next page.)
Fig. 3 Cross-spectra of pressure variations at ocean bottom and of accelerations of seismic oscillations of the ocean bottom registered by DONET stations. (Blue curves are obtained only taking into account vertical acceleration, and red curves take the optimal linear combination of all three acceleration components into account.) The name of the station and the ocean depth at its installation point is indicated above each one of the spectra. The vertical lines correspond to theoretical values of the critical frequencies f_g and f_{ac}, restricting the range of "forced oscillations"

Nosov *et al. Earth, Planets and Space* (2018) 70:100

Page 5 of 13

Nosov *et al. Earth, Planets and Space* (2018) 70:100

Page 6 of 13

$(\omega = 2\pi f)$. This dispersion relation can be written in the following form:

$$k_x = \frac{2\pi}{c}\sqrt{f^2 - f_n^2},$$

where $f_n = c(1 + 2n)/4H$ is a discrete set of normal frequencies. The limit frequency for acoustic waves is the lowest normal frequency (the cutoff frequency): $f_{ac} \equiv f_0 = c/4H$. If $f > f_{ac}$, the value of k_x is real—in this case perturbations created by the source can propagate horizontally like acoustic waves. If $f < f_{ac}$ the value of k_x becomes imaginary, no acoustic waves arise in this case, and perturbations die out exponentially as the distance from the source increases. However, at frequencies close to the cutoff frequency, i.e., at the higher-frequency end of the forced oscillation band, certain manifestations of water compressibility may be observed at insignificant distances from the source.

Spectral analysis of pressure variations and vertical accelerations

Cross-spectral analysis only shows the fact that pressure variations are proportional to the vertical component of acceleration. To check how accurately formula (1) actually holds true can be done with the aid of spectral analysis. Figure 4 presents power spectra of pressure variations (green curves) and of the vertical component of acceleration (violet curves). The acceleration is preliminarily multiplied by the quantity ρH so as to be presented in units of pressure. The density of water ρ was set equal to 1030 kg/m^3, the value of H was chosen equal to the ocean depth at the installation point of the observatory. The analysis was also performed applying Welch averaging with the same segment size (2^{13}) and overlap (50%). The limit frequencies f_g and f_{ac} confining the range of forced oscillations are shown by black vertical lines, and the 95% confidence interval is shown in the left upper corner.

The spectral curves within the range of forced oscillations are shown in Fig. 4 to be either totally identical or exhibit very similar behaviours, up to the repetition of minor peculiarities in the spectrum. Noticeable differences are observed in the case of observatories B06, C09, E18, and, to a somewhat lesser degree of B08. We recall that in the case of observatories B06, B08 and C09, located close to submarine slopes, the cross-spectra also

showed a certain disagreement between the pressure variations and vertical acceleration.

The difference in the spectra from observatory E18 deserves a special comment. In this case, the cross-spectrum (see Fig. 3) practically exhibits perfect proportionality between pressure and acceleration. Moreover, the fine structure of spectral curves within the range of forced oscillations is shown in Fig. 4 to be actually identical. Only the signal level is different (by a factor of about 1.7). Such a significant error in determining the value of ρH is quite improbable. Uncertainty in the calibration of a pressure gauge is also to be excluded, as shown by the joint analysis of PG data from all 10 observatories (Nurislamova and Nosov 2016). Most likely, this case was due to an error in the calibration of accelerometers of observatory E18. Simple visual comparison of the respective spectra of signals, registered by observatories E18 and E17, can serve as an additional argument in favour of this assumption. The distance between these observatories (12.4 km) is quite inferior to their distance from the source (750 km). Consequently, the signals registered by E18 and E17 should not be expected to differ significantly. From Fig. 4, it is well seen that the pressure spectra are indeed characterized by identical levels. At the same time, the acceleration spectrum for E18 exhibits a noticeably lower level.
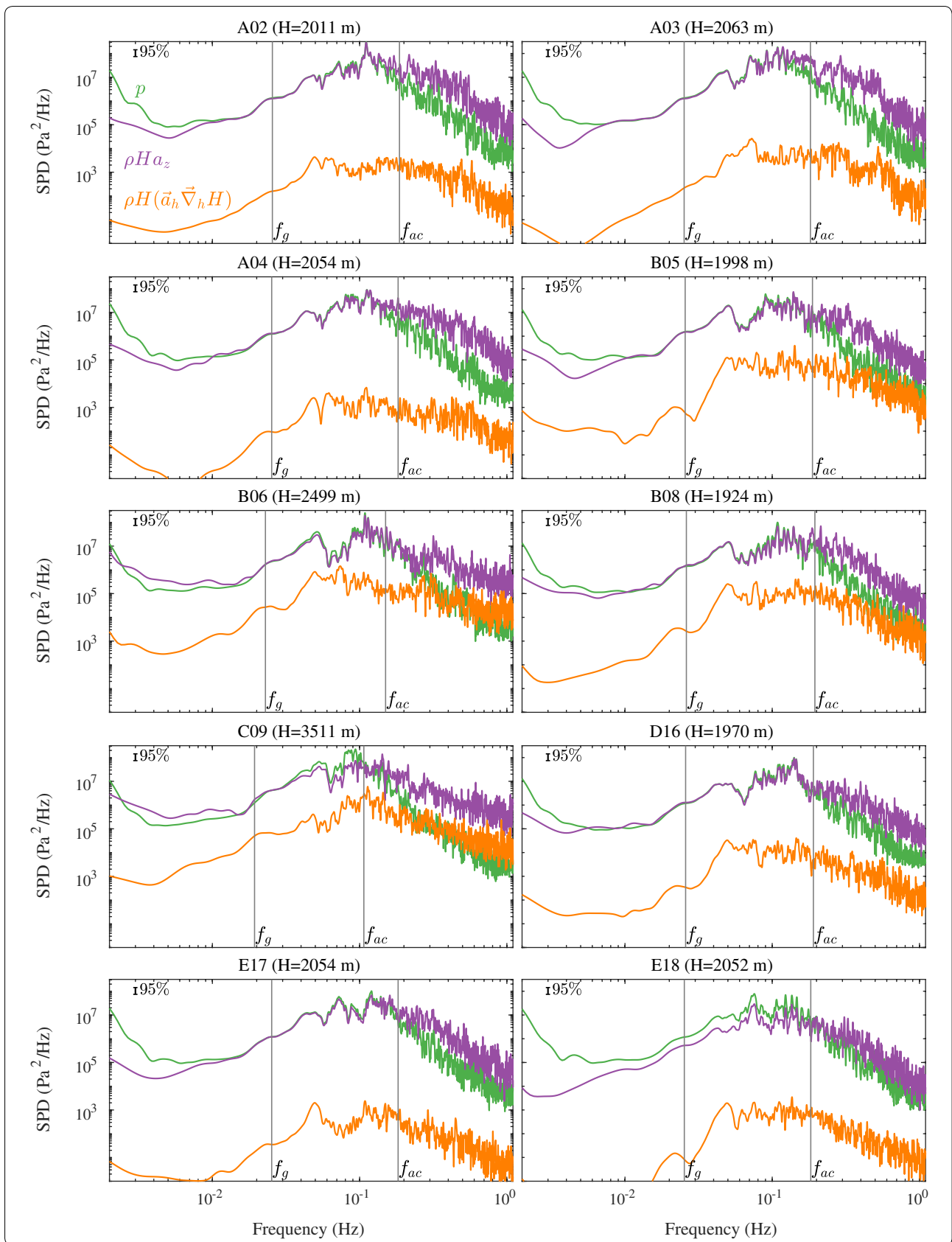
Comparison of the spectra of pressure variations at the ocean bottom and vertical accelerations of the ocean bottom motion can be applied in practice for testing the calibration precision of sensors in situ. It is remarkable that in the case of such a test there is no need to make use of data on the water density and the ocean depth. It is sufficient to take advantage of accurate measurements of the total pressure at the ocean bottom, P. The average value of the total pressure $\overline{P}$ and the value of ρH, that represents the mass of a water column of unit area, are related by the obvious formula $\overline{P} = \rho H g$. Using it to derive the quantity ρH and further substituting it into formula (1), we obtain an expression that is convenient for use in practice,

$$p = a_z \overline{P}/g.$$

In Table 1, the measured values of $\overline{P}$ and the calculated values of $\rho H g$ ($\rho = 1030$ kg/m^3, $g = 9.8$ m/s^2) are compared for each of the 10 observatories. The relative

(See figure on next page.)

Fig. 4 Power spectra of pressure variations at ocean bottom (green line) and of the contributions of vertical (violet line) and horizontal (orange line) components of acceleration to variations in the near-bottom pressure. The name of a station and the ocean depth at its location point is indicated above each one of the spectra. The vertical lines correspond to theoretical values of the critical frequencies f_g and f_{ac}, restricting the range of "forced oscillations". The 95% confidence interval is shown in the left upper corner of each plot

Nosov *et al. Earth, Planets and Space* (2018) 70:100

Page 7 of 13

Nosov *et al. Earth, Planets and Space* (2018) 70:100

Page 8 of 13

difference in the values of $\overline{P}$ and of ρHg is seen not to exceed fractions of a percent. This points to a good precision in the determination of ocean depths and to the assumption concerning the water density to be correct.

Contribution of horizontal movements of the ocean bottom to near-bottom pressure variations

For theoretical analysis of the properties of a pressure field induced in the ocean by the ocean bottom undergoing seismic movements of small amplitude, we shall consider a layer of ideal homogeneous compressible liquid of variable depth in the field of gravity. We shall place the origin of the rectangular coordinate system at the unperturbed water surface. The $0z$-axis is directed vertically upward, while the $0x$- and $0y$-axes are horizontal (eastward and northward, respectively). Taking into account of the assumptions made, the equations of hydrodynamics reduce to the classical wave equation supplemented with boundary conditions at the free surface and on the ocean bottom (Levin and Nosov 2016; Landau and Lifshitz 1987).

$$\frac{1}{c^2}\frac{\partial^2 F}{\partial t^2} - \Delta F = 0, \tag{2}$$

$$\frac{\partial^2 F}{\partial t^2} + g\frac{\partial F}{\partial z} = 0 \quad for\ z = 0, \tag{3}$$

$$\frac{\partial F}{\partial \vec{n}} = (\vec{v}_b, \vec{n}) \quad for\ z = -H(x,y), \tag{4}$$

where F is the velocity potential of the flow, $\vec{v}_b$ is the velocity vector of the ocean bottom motion, $\vec{n} \equiv (n_x, n_y, n_z)$ is the normal to the bottom surface with components determined by the following formulas:

$$n_x = \frac{\frac{\partial H}{\partial x}}{\sqrt{\left(\frac{\partial H}{\partial x}\right)^2 + \left(\frac{\partial H}{\partial y}\right)^2 + 1}},$$

$$n_y = \frac{\frac{\partial H}{\partial y}}{\sqrt{\left(\frac{\partial H}{\partial x}\right)^2 + \left(\frac{\partial H}{\partial y}\right)^2 + 1}}, \tag{5}$$

$$n_z = \frac{1}{\sqrt{\left(\frac{\partial H}{\partial x}\right)^2 + \left(\frac{\partial H}{\partial y}\right)^2 + 1}}.$$

The field of dynamic pressure is related to the potential by the following formula:

$$p = -\rho\frac{\partial F}{\partial t}. \tag{6}$$

The response of a layer of liquid to movements of the ocean bottom, described by Eqs. (2)–(4), involves gravity surface waves, acoustic waves and forced oscillations. In the general case, all three physical phenomena coexist in time and space, and they all induce pressure variations at the ocean bottom. Gravity and acoustic waves are capable of propagating both along their source and outside it. Therefore, the contribution of waves to pressure at the ocean bottom depends, besides the properties of their source, also on the properties of the propagation path of the waves. Contrary to waves, forced oscillations are directly connected with the site of the source and the time of its activity. Consequently, the contribution of forced oscillations to pressure variations depends exclusively on the properties of the source.

The equations for describing forced oscillations can be derived from the set of Eqs. (2)–(4), if the compressibility of water and the force of gravity are neglected

Table 1 Average values of the total pressure $\overline{P}$ versus the values of ρHg ($\rho = 1030$ kg/m³, $g = 9.8$ m/s²), σ_P is the standard deviation of the total pressure P

Observatory	Ocean depth (m)	$\overline{P} \pm \sigma_P$ (kPa)	ρHg (kPa)	$(\rho Hg - \overline{P})/(\rho Hg)$ %
KMA02	2011	20374.2 ± 3.4	20319.7	− 0.2678
KMA03	2063	20886.0 ± 3.6	20845.2	− 0.1959
KMA04	2054	20804.6 ± 2.9	20754.2	− 0.2428
KMB05	1998	20206.6 ± 2.6	20188.4	− 0.0902
KMB06	2499	25255.8 ± 3.1	25250.6	− 0.0204
KMB08	1924	19466.5 ± 2.6	19440.7	− 0.1329
KMC09	3511	35447.4 ± 3.8	35476.2	0.0812
KMD16	1970	19967.0 ± 2.8	19905.5	− 0.3090
KME17	2054	20811.6 ± 3.0	20754.2	− 0.2767
KME18	2052	20757.1 ± 2.7	20734.0	− 0.1111

Nosov *et al. Earth, Planets and Space* (2018) 70:100

Page 9 of 13

$(c = \infty, g = 0)$. Transforming, with the aid of formula (6), potential to pressure in the equations we obtain

$$\Delta p = 0, \tag{7}$$

$$p = 0 \quad for \ z = 0, \tag{8}$$

$$\frac{\partial p}{\partial \vec{n}} = -\rho(\vec{a}_b, \vec{n}) \quad for \ z = -H(x, y), \tag{9}$$

where $\vec{a}_b \equiv (a_x, a_y, a_z)$ is the vector of the ocean bottom acceleration.

For an ocean of constant depth $(H(x, y) = const)$ the normal vector is of the form $\vec{n} \equiv (0, 0, 1)$. In this case, the contribution to pressure variations is evidently given only by the vertical component a_z. If the a_z component is independent of horizontal coordinates, then the pressure does also not depend on horizontal coordinates, and the only possible solution of the Laplace equation (7) is a linear function: $p(x, y, z) = C_1 z + C_2$, where C_1 and C_2 are constants of integration. Upon satisfying boundary conditions (8) and (9), we obtain

$$p = -\rho a_z z. \tag{10}$$

The pressure at the ocean bottom (at $z = -H$), calculated by formula (10), corresponds precisely to the value determined by formula (1).

Let us further consider an ocean of variable depth. If the slopes are small, then the change in dynamic pressure in the liquid along the normal $\vec{n}$ to the ocean bottom is determined by the linear function $p = C_1 \xi + C_2$, where ξ is the coordinate counted down from the water surface along the normal to the ocean bottom. Determining the constants of integration from boundary conditions (8) and (9), we obtain

$$p = -\rho(\vec{a}_b, \vec{n})\xi. \tag{11}$$

For the pressure at the ocean bottom (at $\xi = -\frac{H}{n_z}$) formula (11) gives

$$p = \rho(\vec{a}_b, \vec{n})\frac{H}{n_z} = \rho H((\vec{a}_h, \vec{\nabla}_h H) + a_z),$$
$$(\vec{a}_h, \vec{\nabla}_h H) = a_x \frac{\partial H}{\partial x} + a_y \frac{\partial H}{\partial y}, \tag{12}$$

where $\vec{a}_h = (a_x, a_y)$ is the horizontal acceleration vector, and the operator $\vec{\nabla}_h$ operates in the horizontal plane.

From expression (12), it follows that, if there exists a depth gradient, then the horizontal components of acceleration are capable of providing an additional contribution to pressure at the ocean bottom. The contribution of horizontal components is proportional to the inclination of the bottom, which actually rarely exceeds 0.1. Consequently, in spite of horizontal components of acceleration in seismic waves usually being greater than the vertical

components (Fig. 2), the contribution of horizontal accelerations to pressure variations is not to be expected to be dominant.

The orange curves in Fig. 4 show the power spectra of the contribution of the horizontal components of acceleration to variations in the near-bottom pressure estimated as $\rho H(\vec{a}_h, \vec{\nabla}_h H)$. From the figure, it can be seen that within the "forced oscillations" band the contribution of horizontal acceleration components is always inferior to the contribution of the vertical component (violet curves). Here, in many cases the orange and violet curves are at distances differing by over 3–4 orders of magnitude, which is evidence of the negligibly small role of horizontal accelerations in the formation of near-bottom pressure variations. The smallest distance between the orange and violet curves (less than 0.5 an order of magnitude) is observed for the observatory B06. It is remarkable that, here, the maximum of the spectrum of the orange curve coincides with a local minimum of the violet curve. From our point of view, precisely this peculiarity explains the localized in frequency deviation, observed in Fig. 3, of MSC from unity. In the case of observatories B08 and C09, the orange and violet curves approach each other at a distance inferior to one order of magnitude, in the case B05—less than 1.5 orders of magnitude. The "defects" of cross-spectra are quite noticeable in Fig. 3 in the case of these observatories.

In accordance with formula (12), the horizontal components of acceleration for all points, lying on a horizontal bottom, should provide a zero contribution to the variations of pressure. But, if an area of the horizontal bottom is situated close to an underwater slope, this contribution may turn out to differ from zero. Let us estimate the long-range action of a localized source of pressure variations. To this end, we consider harmonic oscillations of an axial-symmetric segment of the ocean bottom in a basin of constant depth.

$$a_z(r, t) = a_0(r)e^{i\omega t}, \tag{13}$$

where $r = \sqrt{x^2 + y^2}$ is the distance from the center of the oscillating segment, $a_0(r)$ is a function describing the distribution of accelerations in space, ω is the cyclic frequency of oscillations.

Solution of the problem (7)–(9) for an axial-symmetric source (13) can be found analytically with the aid of the Fourier–Bessel transformation

$$p(r, z, t) = -\rho e^{i\omega t} \int_0^\infty \frac{X(k) \sinh(kz) J_0(kr)}{\cosh(kH)} dk, \tag{14}$$

$$X(k) = \int_0^\infty r a_0(r) J_0(kr) dr, \tag{15}$$

Nosov *et al. Earth, Planets and Space* (2018) 70:100

Page 10 of 13

where J_0 is the Bessel function of the first kind of zeroth order.

Let us choose the most simple form for the oscillating segment of the ocean bottom,

$$a_0(r) = A_0\theta(R - r), \tag{16}$$

where R is the radius of the oscillation source, A_0 is the acceleration amplitude, θ is the Heaviside function. In this case, the integral (15) is readily calculated analytically,

$$X(k) = \frac{A_0 R J_1(kR)}{k}. \tag{17}$$

The resultant formula for calculating pressure at the ocean bottom has the following form:

$$p(r, -H, t) = A_0\rho H e^{i\omega t} \int\limits_0^\infty \frac{\hat{R}J_0(\hat{k}\hat{r})J_1(\hat{k}\hat{R})\tanh(\hat{k})}{\hat{k}} d\hat{k}, \tag{18}$$

where the integrand involves the dimensionless variables $\hat{R} = \frac{R}{H}, \hat{r} = \frac{r}{H}$ and $\hat{k} = kH$. From formula (18), the amplitude of pressure variations is seen to be always proportional to the quantity $A_0\rho H$, while the character of the decrease in pressure with distance is determined by the integral.

The results of numerical calculation of the integral are presented in Fig. 5. The decrease in the influence on slope with pressure is seen, independently of the source radius, to be exponentially rapid as the distance from the boundary of the source increases. At a distance from the boundary of the source, equal to one ocean depth, the pressure amplitude is reduced by approximately one order of magnitude. Consequently, a gauge at the ocean bottom effectively registers pressure variations, due to bottom oscillations, within a radius that does not exceed 1–2 ocean depths. It is remarkable that the size of the segment giving the most significant contribution to pressure variations is significantly less than the lengths of seismic waves. Indeed, in the case of a maximum frequency of forced oscillations between 0.02 and 0.1 Hz and a velocity of surface seismic waves of 2–4 km/s (An et al. 2017), the wavelengths vary between 20 and 200 km. Consequently, the region contributing to pressure variations can be assumed to move as a single whole.

The circular marks of radii equal to 1, 2, and 3 ocean depths are shown in Fig. 1 at the installation points of each of the DONET observatories. Observatories B06 and C09 are clearly seen to have steep slopes at a distance of 1–2 ocean depths. In the case of other observatories, the bottom slopes within a radius of 2 ocean depths are insignificant.
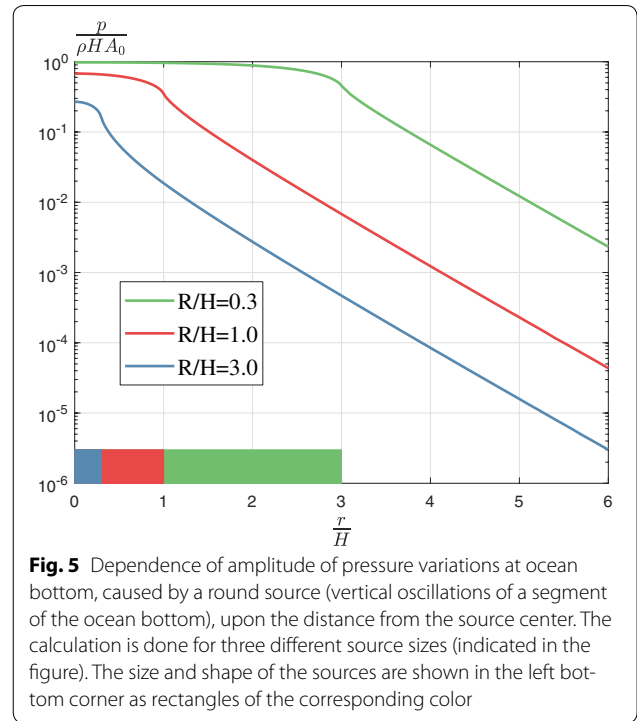

Fig. 5 Dependence of amplitude of pressure variations at ocean bottom, caused by a round source (vertical oscillations of a segment of the ocean bottom), upon the distance from the source center. The calculation is done for three different source sizes (indicated in the figure). The size and shape of the sources are shown in the left bottom corner as rectangles of the corresponding color

If our reasoning and, in particular, formula (12) is correct, there should exist a linear combination of time series of acceleration components, $G_x a_x + G_y a_y + a_z$, possessing a "perfect" cross-spectrum with pressure. An "ideal" cross-spectrum implies MSC=1 within the frequency band of "forced oscillations". All deviations from the "ideal case" evidently reduce the MSC value. For this reason, we shall consider the following integral to be the measure of a cross-spectrum being "ideal":

$$I = \int\limits_{f_g}^{f_{ac}} MSC(f, G_x, G_y) df, \tag{19}$$

where MSC is the magnitude-squared coherence of variations of the pressure p and of the quantity $a_x G_x + a_y G_y + a_z$. If these values exhibit "ideal" proportionality ($p \sim a_x G_x + a_y G_y + a_z$), the integral is equal to its maximum value. The coefficients G_x and G_y were determined from the condition that the integral I be equal to its maximum value. In determining the coefficients G_x and G_y use was made of the downhill simplex method.

Cross-spectra for the ideal combinations found are presented in Fig. 3 by red curves. From the figure, it is seen that the MSC and PL "defects" (blue curves) can indeed by corrected by taking into account the horizontal

Nosov *et al. Earth, Planets and Space* (2018) 70:100

Page 11 of 13

components of acceleration. The values of quantities G_x and G_y thus obtained can be interpreted as the weighted-mean components of ocean depth gradient in the region adjacent to the given observatory. The weighted-mean bottom slopes calculated as $\sqrt{G_x^2 + G_y^2}$ are shown in Table 2. The values obtained of $\sqrt{G_x^2 + G_y^2}$ are in reasonable agreement with the depth gradients within the regions considered that were estimated on the basis of J-EGG500 data (see Fig. 1).

Conclusions

Records provided by the pressure gauges and three-component accelerograms of ten deep-water DONET observatories in operation during the Great East Japan Earthquake and tsunami of March 11, 2011, have been analyzed. A cross-spectral analysis has shown that a frequency range of "forced oscillations" exists for each observatory, within which pressure variations and the vertical component of acceleration happen to be proportional to each other with a good accuracy. Comparison of the power spectra of signals shows that the proportionality coefficient is actually the mass of a water column of unit area (the product of the water density and the ocean depth) at the installation point of an observatory (Eq. 1). The linear relationship between quantities p and a_z is a direct consequence of Newton's second law applied in the case of a column of liquid of unit cross section, which, being directly connected to the ocean bottom, undergoes vertical forced oscillations as a rigid body.

In the general case, when seismic motions of the bottom take place in the real ocean, not only forced oscillations are generated, but also gravity and acoustic waves, the contribution of which to pressure variations at the ocean bottom violates the linear relationship between quantities p and a. However, the manifestation of gravity waves in pressure variations at the ocean bottom is limited by a maximum limit frequency $f_g = 0.366\sqrt{\frac{g}{H}}$. And, the existence of hydroacoustic waves is restricted by a minimum limit frequency $f_{ac} = \frac{c}{4H}$. Therefore, forced oscillations are realized in a pure form within the frequency band $f_g < f < f_{ac}$, while the linear relationship $p = \rho H a_z$ is clearly observed in cross-spectra and in power spectra of the signals. Theoretical values of the limit frequencies f_g and f_{ac} are quite consistent with the observed boundaries of the forced oscillation band. The clear relationship observed between pressure variations of the ocean bottom and the vertical component of acceleration makes possible its utilization as a convenient way for mutual verification of pressure gauges and accelerometers in situ.

In the case of observatories installed in regions close to submarine slopes, cross-spectra within the range of

Table 2 Weighted-mean bottom slopes calculated as $\sqrt{G_x^2 + G_y^2}$

Observatory	$\sqrt{G_x^2 + G_y^2}$
KMA02	0.0178
KMA03	0.0446
KMA04	0.0276
KMB05	0.0238
KMB06	0.0619
KMB08	0.0555
KMC09	0.0710
KMD16	0.0089
KME17	0.0249
KME18	0.0543

"forced oscillations" exhibit insignificant deviations of MSC from unity and of PL from zero. From our point of view, such deviations can be caused by a sole source, namely the horizontal movements of submarine slopes, contributing to the pressure variations. For verification of this hypothesis, we obtained a set of equations describing the pressure field in forced oscillations of a water layer in a basin of variable depth. On the basis of this set, a formula was obtained that relates pressure variations at the ocean bottom and acceleration components in the case of a gently sloping ocean bottom (Eq. 12).

From the formula, it is seen that in the case of observatories, situated in nearly horizontal segments of the ocean bottom, the dominant contribution to the pressure is due to the vertical component of acceleration.

An analytical solution is obtained for the problem of a pressure field, caused by harmonic oscillations of a segment of the ocean bottom within the frequency band of "forced oscillations." On the basis of this solution, the amplitude of pressure variations is shown to undergo a rapid exponential drop with an increase in the distance from the source. Therefore, in the case of observatories installed on a nearly horizontal bottom a contribution to the pressure variations can only be given by submarine slopes the distance from which does not exceed 1–2 ocean depths. A cross-spectral analysis of pressure variations and of three-component accelerograms have confirmed the hypothesis concerning the contribution of horizontal movements of nearby submarine slopes to pressure variations.

Nosov *et al. Earth, Planets and Space* (2018) 70:100

Page 12 of 13

Meteorological Agency; MSC: magnitude-squared coherence; NEPTUNE: The Canadian North-East Pacific Underwater Networked Experiments (NEPTUNE-Canada); OBS: ocean bottom seismometer; PL: phase lag; PG: pressure gauge; SPD: spectral power distribution.

Author details
[1] Chair of Physics of Sea and Inland Water, Faculty of Physics, M.V.Lomonosov Moscow State University, Moscow, Russia 119991. [2] Institute of Marine Geology and Geophysics, Far Eastern Branch of Russian Academy of Sciences, Nauki 1B, Yuzhno-Sakhalinsk, Russia 693022. [3] Japan Agency for Marine-Earth Science and Technology (JAMSTEC), 2-15 Natsushima, Yokosuka 237-0061, Japan. [4] Institute of Education, Research and Regional Cooperation for Crisis Management, Kagawa University, 1-1 Saiwai-cho, Takamatsu 760-8521, Japan.

Competing interests
The authors declare that they have no competing interests.

Availability of data and materials
The DONET data are obtained according to the Implementing Agreement between Faculty of Physics of Lomonosov Moscow State University and JAMSTEC, which does not imply transfer to a third Party.

Consent for publication
Not applicable.

Ethics approval and consent to participate
Not applicable.

Publisher's Note
Springer Nature remains neutral with regard to jurisdictional claims in published maps and institutional affiliations.

References
An C, Cai C, Zheng Y, Meng L, Liu P (2017) Theoretical solution and applications of ocean bottom pressure induced by seismic seafloor motion. Geophys Res Lett 44(20):10272–10281. https://doi.org/10.1002/2017GL075137

Araki E, Yokobiki T, Kawaguchi K, Kaneda Y (2013) Background seismic noise level in donet seafloor cabled observation network. In: 2013 IEEE international underwater technology symposium (UT), pp 1–4. https://doi.org/10.1109/UT.2013.6519858. IEEE

Barnes CR, Team NC (2007) Building the world's first regional cabled ocean observatory (neptune): realities, challenges and opportunities. OCEANS 2007:1–8. https://doi.org/10.1109/OCEANS.2007.4449319

Bendat JS, Piersol AG (2010) Random data: analysis and measurement procedures. Wiley series in probability and statistics, 4th edn. Wiley, Hoboken

Bloomfield P (2000) Fourier analysis of time series: an introduction. Wiley series in probability and statistics. Applied probability and statistics section, 2nd edn. Wiley, New York

Bolshakova A, Inoue S, Kolesov S, Matsumoto H, Nosov M, Ohmachi T (2011) Hydroacoustic effects in the 2003 tokachi-oki tsunami source. Russ J Earth Sci 12(2):1–14. https://doi.org/10.2205/2011ES000509

Bradner H (1964) Seismic measurements on the ocean bottom. Science 146(3641):208–216

Ewing M, Vine A (1938) Deep-sea measurements without wires or cables. Eos Trans Am Geophys Union 19(1):248–251. https://doi.org/10.1029/TR019I001P00248

Favali P, Beranzoli L (2009) Emso: European multidisciplinary seafloor observatory. Nucl Instrum Methods Phys Res Sect A 602(1):21–27. https://doi.org/10.1016/j.nima.2008.12.214

Filloux JH (1983) Pressure fluctuations on the open-ocean floor off the gulf of california: tides, earthquakes, tsunamis. J Phys Oceanogr 13(5):783–796

Gusman AR, Sheehan AF, Satake K, Heidarzadeh M, Mulia IE, Maeda T (2016) Tsunami data assimilation of cascadia seafloor pressure gauge records from the 2012 haida gwaii earthquake. Geophys Res Lett 43(9):4189–4196. https://doi.org/10.1002/2016GL068368

Jaque VN, Soloviev SL (1971) Distant registration of tsunami type weak waves on the shelf of kuril islands. Doklady USSR Acad Sci Earth Sci Sect 198(4):816–817 [In Russian]

JMA: Japan Meteorological Agency. http://www.jma.go.jp/jma/en/2011_Earthquake/Information_on_2011_Earthquake.html. Accessed 31 Jan 2018

Kaneda Y (2010) The advanced ocean floor real time monitoring system for mega thrust earthquakes and tsunamis-application of donet and donet2 data to seismological research and disaster mitigation. In: OCEANS 2010, pp 1–6. https://doi.org/10.1109/OCEANS.2010.5664309 IEEE

Landau LD, Lifshitz EM (1987) Fluid mechanics. In: Course of theoretical physics, 2nd edn, vol. 6. Pergamon Press. Oxford, England, New York

Levin BW, Nosov MA (2016) Physics of tsunamis, 2nd edn. Springer, Cham, p 388. https://doi.org/10.1007/978-3-319-24037-4

Li W, Yeh H, Hirata K, Baba T (2009) Ocean-bottom pressure variations during the 2003 tokachi-oki earthquake. In: Nonlinear wave dynamics: Selected papers of the symposium held in honor of Philip LF Liu's 60th Birthday, pp 109–126. https://doi.org/10.1142/9789812709042_0005. World Scientific

Matsumoto H, Nosov MA, Kolesov SV, Kaneda Y (2017) Analysis of pressure and acceleration signals from the 2011 tohoku earthquake observed by the donet seafloor network. J Disaster Res 12(1):163–175. https://doi.org/10.20965/jdr.2017.p0163

Nakano M, Tonegawa T, Kaneda Y (2012) Orientations of DONET seismometers estimated from seismic waveforms. JAMSTEC Rep Res Dev 15:77–89 [In Japanese]

Nosov MA, Grigorieva SS (2015) Tsunami forecasting based on deepwater-station data. Mosc Univ Phys Bull 70(4):326–332. https://doi.org/10.3103/S002713491504013X

Nosov MA, Kolesov SV (2007) Elastic oscillations of water column in the 2003 tokachi-oki tsunami source: in-situ measurements and 3-d numerical modelling. Nat Hazards Earth Syst Sci 7(2):243–249

Nosov MA, Kolesov SV, Ostroukhova AV, Alekseev AB, Levin BW (2005) Elastic oscillations of the water layer in a tsunami source. Dokl Earth Sci 404(7):1097–1100 Springer

Nurislamova GN, Nosov MA (2016) The horizontal motion of a water layer during the passage of tsunami waves based on data from a dense ocean-floor network of deepwater sea-level stations. Mosc Univ Phys Bull 71(5):520–525. https://doi.org/10.3103/S0027134916050143

Ohmachi T, Inoue S (2010) Dynamic tsunami generation process observed in the 2003 Tokachi-oki, Japan, earthquake. World Scientific, Singapore, pp 159–168. https://doi.org/10.1142/9789812838148_0009

Rabinovich AB, Eblé MC (2015) Deep-ocean measurements of tsunami waves. Pure Appl Geophys 172(12):3281–3312. https://doi.org/10.1007/s00024-015-1058-1

Soloviev SL (1968) The tsunami problem and its importance for Kamchatka and the Kuril Islands. The tsunami problem. Nauka 19:7–50 [In Russian]

Suetsugu D, Shiobara H (2014) Broadband ocean-bottom seismology. Annu Rev Earth Planet Sci 42:27–43

Nosov *et al. Earth, Planets and Space* (2018) 70:100

Page 13 of 13

Takahashi N, Imai K, Ishibashi M, Sueki K, Obayashi R, Tanabe T, Tamazawa F, Baba T, Kaneda Y (2017) Real-time tsunami prediction system using donet. J Disaster Res 12(4):766–774. https://doi.org/10.20965/jdr.2017.p0766

Titov V, Rabinovich AB, Mofjeld HO, Thomson RE, González FI (2005) The global reach of the 26 december 2004 sumatra tsunami. Science 309(5743):2045–2048. https://doi.org/10.1126/science.1114576

Tolstoy I (1987) Ocean acoustics: theory and experiment in underwater sound, 2nd edn. Acoustical Society of America by the American Institute of Physics, New York

Watanabe O, Matsumoto H, Sugioka H, Mikada H, Suyehiro K, Otsuka R (2004) Offshore monitoring system records recent earthquake off japan's northernmost island. Eos Trans Am Geophys Union 85(2):14–15. https://doi.org/10.1029/2004EO020003

Webb SC (1998) Broadband seismology and noise under the ocean. Rev Geophys 36(1):105–142